Macromolecules

Article

pubs.acs.org/Macromolecules

Polystyrene-*block*-poly(ethylene oxide) Bottlebrush Block Copolymer Morphology Transitions: Influence of Side Chain Length and Volume Fraction

Yue Gai, Dong-Po Song, Benjamin M. Yavitt, and James J. Watkins*

Department of Polymer Science and Engineering, University of Massachusetts Amherst, 120 Governors Drive, Amherst, Massachusetts 01003, United States

Supporting Information

ABSTRACT: A systematic study was conducted to investigate the morphology transitions that occur in polystyrene-*block*-poly(ethylene oxide) (PS-*b*-PEO) bottlebrush block copolymers (BBCP) upon varying PEO volume fraction (f_{PEO}) from 22% to 81%. A series of PS-*b*-PEO BBCPs with different PEO side chain lengths were prepared using ring-opening metathesis polymerization (ROMP) of PEO−norbornene (PEO-NB) (M_n ∼ 0.75, 2.0, or 5.0 kg/mol) and PS−norbornene (PS-NB) (M_n ∼ 3.5 kg/mol) macromonomers (MM). A map of f_{PEO} versus side chain asymmetry (M_n(PEO-NB)/M_n(PS-NB)) was constructed to describe the BBCP phase behavior. Symmetric and asymmetric lamellar morphologies were observed in the BBCPs over an exceptionally wide range of f_{PEO} from 28% to 72%. At high f_{PEO}, crystallization of PEO was evident. Temperature-controlled SAXS and WAXS revealed the presence of high order reflections arising from phase segregation above the PEO melting point. A microphase transition temperature T_{MST} was observed over a temperature range of 150−180 °C. This temperature was relatively insensitive to both side chain length and volume fraction variations. The findings in this study provide insight into the rich phase behavior of this relatively new class of macromolecules and may lay the groundwork for their use as templates directing the fabrication of functional materials.

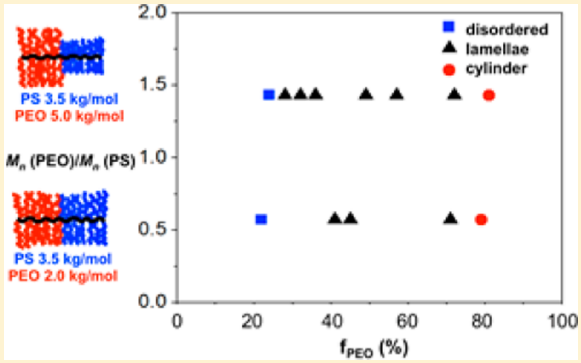

INTRODUCTION

Block copolymers (BCPs) have attracted tremendous attention due to their roles as scaffolds in directing self-assembly from a few to tens of nanometers through microphase separation.[1−15] For a traditional linear A−B block copolymer, the morphology is governed by control over the Flory−Huggins parameter (χ), the number of repeat units (N) and the block volume fraction (f).[1,3,5] Bottlebrush block copolymers (BBCP) are novel architected macromolecules with densely grafted branches attached to a linear backbone.[16,17] Significant repulsive forces between the short densely grafted side chains induce the stretching in the backbone of BBCP, and the BBCPs exhibit a reduced degree of chain entanglement compared to linear BCPs.[18,19] Such intrinsic properties enable BBCP to exhibit fast ordering dynamics with large domain spacings (d-spacings) over 100 nm, offering opportunities for rapid and scalable manufacturing for various applications.[20−30]

Knowledge of BBCP phase behavior is essential for the control of their morphology and subsequent applications. Multiple parameters including the chemical incompatibility of two blocks, the block volume ratio, the side chain asymmetry, and the length of backbone should be considered when investigating their morphology transitions. Theodorakis[31] and co-workers reported a simulation result for the self-assembly of BBCPs in which the transition from lamellae to hexagonally packed cylinders did not quite depend on asymmetry of volume fraction, but rather from the asymmetry of the side chain. This result significantly deviated from the current understanding of linear BCP phase behavior.

Recent experimental studies have offered a glimpse into the phase behavior of BBCPs but not yet provided a satisfactory description of the parameters that precisely control the morphology upon microphase segregation.[32−35] To date there has been incomplete control over molecular characteristics of synthesized BBCP, and studies have been limited to the purely symmetric system. The most developed "graft from" or "graft onto" methods for BBCP synthesis introduced subsequent growth of side chains from a linear backbone, requiring orthogonal mechanisms or the purification of unreacted side chain in grafting process.[36−42] For example, Rzayev's group[20,32] reported the self-assembly of asymmetric polystyrene-*b*-polylactide (PS-*b*-PLA) or polystyrene-*b*-poly(methyl methacrylate) (PS-*b*-PMMA) BBCPs using the "RAFT-ATRP" method, in which they observed the formation of cylindrical structures with 55 nm in average pore size. However, the limited initiation efficiency of macroinitiators could not

Received: July 1, 2016
Revised: January 31, 2017
Published: February 13, 2017

DOI: 10.1021/acs.macromol.6b01415
Macromolecules 2017, 50, 1503−1511

guarantee complete grafting in most "graft-from" or "graft to" methods, making it difficult to determine side chain characteristics and precisely explain the control over the BBCP phase transition.[19]

On the other hand, combinations of norbornene (NB)-modified macromonomers (MM) and ring-opening metathesis polymerization (ROMP) developed by Xia et al.[19,43] and other groups[44,45] presented a more attractive route to synthesize BBCP, ensuring complete grafting of every backbone repeat unit. Nevertheless, only lamellar structure of BBCP[18,43,46] in symmetric system has been investigated in detail so far. For instance, Gu et al.[18] and Dalsin et al.[46] separately revealed phase segregation of symmetric PS-*b*-PLA or polystyrene-*b*-(atactic) polypropylene (PS-*b*-aPP) BBCPs with well-ordered lamellae over a wide range of domain sizes. While those works explored the relationship between backbone length and the resulting domain spacing, there were no complete studies of the role of block volume fraction or side chain length on the phase behavior of asymmetric BBCPs, especially the BBCPs synthesized via MM methods.

Here we report the morphology transitions of polystyrene-*b*-poly(ethylene oxide) (PS-*b*-PEO) BBCP as a function of PEO side chain length and block volume fraction (Figure 1). We

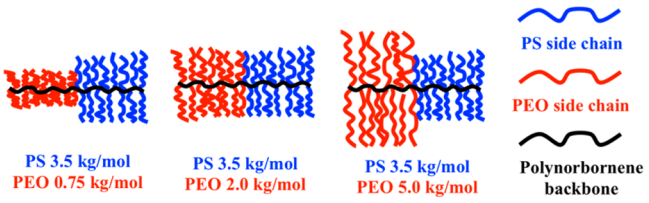

Figure 1. Illustration of PS-*b*-PEO BBCP with designated side chain lengths: PEO-NB (M_n ~ 0.75, 2.0, and 5.0 kg/mol accordingly) and PS-NB (M_n ~ 3.5 kg/mol). The PEO volume fraction (f_{PEO}) was controlled approximately from 20% to 80%.

specifically studied the asymmetric architectures, crystallization effects on microphase segregation, and microphase transition temperature (T_{MST}). Understanding of the role that side chain length and block volume fraction play in controlling the phase behavior of BBCP offers new opportunities for creating functional materials using BBCP as the scaffolds.

EXPERIMENT

Materials. *cis*-5-Norbornene-exo-2,3-dicarboxylic anhydride (95%), ethanolamine (99.0%, ACS grade), triethylamine (>99.5%), *N*,*N*′-dicyclohexylcarbodiimide (DCC, >99.0%), 4-(dimethylamino)pyridine (DMAP, >99%), sodium azide (NaN_3, >99.5%), styrene (contained 4-*tert*-butylcatechol as stabilizer, ≥99%), CuBr (98%), ethyl 2-bromoisobutyrate (98%), *N*,*N*,*N*′,*N*″,*N*″-pentamethyldiethylenetriamine (PMDETA, 99%), poly(ethylene glycol) methyl ether (M_n ~ 0.75, 2.0, and 5.0 kg/mol), and exo-5-norbornenecarboxylic acid (97%) were purchased from Sigma-Aldrich. Pentynoicacid (98%), anhydrous dichloromethane (DCM), anhydrous toluene (99.8%), anhydrous *N*,*N*-dimethylformamide (DMF, 99.8%), and anhydrous tetrahydrofuran (THF, 99.9%) were purchased from Acros Organics. Third-generation Grubbs catalyst was prepared based on the reported method.[19] Styrene was passed through basic aluminum oxide before the polymerization. Under nitrogen flow, PEO methyl ether was heated at 120 °C for about 4 h to remove moisture before usage. Ruthenium tetroxide (0.5% stabilized aqueous solution) was purchased from VWR.

Measurements. Proton or carbon nuclear magnetic resonance (^{1}H NMR/^{13}C NMR) spectroscopy was recorded in $CDCl_3$ using a a Bruker 300 or 500 NMR spectrometer. Gel permeation chromatography (GPC) of the BBCPs was carried out in THF on two PLgel 10 μm mixed-B LS columns (Polymer Laboratories) connected in series with a DAWN EOS multiangle laser light scattering (MALLS) detector and an RI detector. A calibration standard of PS with M_n ~ 30 kg/mol was used for the BBCP, and d*n*/d*c* values were obtained for each injection by assuming 100% mass elution from the columns. GPC analyses of PS-NB and PEO-NB MM were carried out using a Polymer Labotatories PL-GPC50 instrument with two 5 μm mixed-D columns, a 5 μm guard column, and a RI detector (HP1047A). THF was used as the eluent at a flow rate of 1.0 mL/min. Polystyrene standards were used for the calibration. Fourier transform infrared (FT-IR) (PerkinElmer 2000) spectra of BBCP were taken in the range from 4000 to 650 cm^{-1} on ATR mode. Differential scanning calorimetry (DSC) analysis was performed on TA Instruments Q200-1390-RCS. The melting enthalpy of PEO domain was measured on the second heating scan from −60 to 110 °C at a rate of 5 °C/min. The heat of fusion for 100% crystalline PEO was ΔH_m^0 ~ 197 J/g as referred in the TA Instruments thermal application note. Morphology and domain spacing of BBCP were characterized using small/wide-angle X-ray scattering (SAXS/WAXS). Bulk films were placed in the center of a metal washer and sealed with Kapton tape. These samples were measured on Ganesha SAXS-LAB with Cu Kα 0.154 nm line on SAXS/WAXS or ESAXS mode with a temperature control stage. Cryomicrotoming (Leica Ultracut microtome) was used to cut the nanocomposite bulk film into 50 nm thin films. Sections were collected using a carbon film supported by copper grids. Subsequent RuO_4 staining was applied to improve contrast between PS and PEO domains. The prepared thin films were then characterized by transmission electron microscopy (TEM) on a JEOL 2000FX (200 kV).

MM Synthesis. The synthesis and characterization of PS-NB (M_n ~ 3.5 kg/mol) and PEO-NB (M_n ~ 0.75, 2.0, and 5.0 kg/mol) followed the established procedures.[19,43,47−50] PS-NB was prepared using atom transfer radical polymerization (ATRP) and click

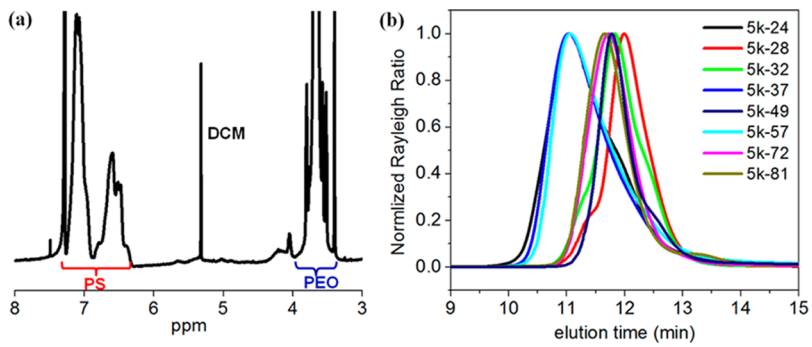

Figure 2. (a) A representative ^{1}H NMR spectrum of PS-*b*-PEO BBCP; signal at 5.32 ppm is ascribed to residue dichloromethane (DCM). (b) GPC MALLS traces of 5k-Y samples.

DOI: 10.1021/acs.macromol.6b01415
Macromolecules 2017, 50, 1503−1511

Table 1. Characteristics of the PS-*b*-PEO BBCP Series (2k-Y and 5k-Y)

BBCP[a]	[Cat.]:[PS_{MM}]:[PEO_{MM}]	f_{PEO}[b] (%)	M_w[c] (kg/mol)	PDI[c]	DP PS[d]	DP PEO[d]	*d*-spacing[e] (nm)
2k-22	1:47:21	22	346.0	1.09	70	34	43.3
2k-41	1:25:31	41	214.6	1.16	30	43	55.6
2k-45	1:38:46	45	393.3	1.38	49	60	82.7
2k-71	1:14:58	71	299.3	1.16	21	92	41.9
2k-79	1:9:61	79	282.9	1.25	14	89	34.4
5k-24	1:100:18	24	714.7	1.28	121	27	43.6
5k-28	1:51:12	28	320.2	1.10	60	16	41.9
5k-32	1:47:14	32	345.9	1.12	60	20	51.1
5k-37	1:101:30	37	727.9	1.26	105	41	46.9
5k-49	1:36:25	49	473.6	1.09	63	42	59.5
5k-57	1:72:50	57	808.0	1.23	81	75	76.2
5k-72	1:20:33	72	416.5	1.13	29	53	35.0
5k-81	1:15:43	81	401.9	1.16	19	56	34.0

[a]BBCPs are labeled as "*X*k-*Y*", where *X* and *Y* represent molecular weight and volume fraction of PEO side chain, respectively. [b]Volume fraction of PEO (f_{PEO}) was calculated using mass ratios of PS and PEO obtained from ^{1}H NMR spectra and approximate bulk densities (1.05 and 1.08 g/cm^3 for PS and PEO, respectively). [c]M_w and PDI were determined by GPC-MALLS. [d]The degree of polymerization was estimated using absolute molecular weights as measured by GPC-MALLS. [e]Domain spacings (*d*-spacings) of BBCPs were calculated using the equation $d = 2\pi/q^*$,where q^* corresponded to the primary peak in SAXS.

chemistry. The synthesis details are provided in the Supporting Information. We specifically describe a simple, high yield strategy to synthesize PEO-NB MM by modifying the end group of commercial available PEO. Under nitrogen flow, PEO methyl ether (CH_3-PEO-OH) was heated at 120 °C for about 4 h to remove moisture. After cooling, 2 mmol of PEO-OH (M_n ~ 0.75 kg/mol (1.5 g), M_n ~ 2.0 kg/mol (4.0 g), or M_n ~ 5.0 kg/mol (10.0 g)), exo-5-norbornene-carboxylic acid (0.55 g, 4 mmol), DCC (0.99 g, 4.8 mmol), and DMAP (24 mg, 0.2 mmol) were added into a 200 mL Schlenk flask followed by 30 mL of anhydrous DCM. The reaction mixture was stirred at room temperature for about 48 h and filtered to remove precipitates, and the filtrate was precipitated in cool diethyl ether three times to yield white solid as PEO-NB. The GPC traces, ^{1}H NMR, ^{13}C NMR spectra, and molecular characteristics of MM are provided in the Supporting Information (Figures S1−S7 and Table S1).

BBCP Preparation through ROMP. In a typical experiment, 40−200 mg of PS-NB and PEO-NB MM were added to separate Schlenk flasks followed by the desired amount of anhydrous DCM. The concentration of the PS-NB MM was controlled from 0.05 to 0.1 M. The resulting solutions were degassed with three cycles of freeze−pump−thaw before the sequential polymerization. At room temperature, the polymerization of PS-NB was initiated by adding the desired amount of third-generation Grubbs catalyst solution in DCM. After the first MM PS-NB reacted for 20 min, solution of the second MM, PEO-NB, was injected into the reaction mixture. This solution was stirred for an additional 2−3 h. The reaction was quenched with ethyl vinyl ether. By tuning the mass ratio of reacting PS-NB and PEO-NB MM, the volume fraction of PS and PEO block was controlled. The mass ratio of PS and PEO block was calculated according to the corresponding molar ratio as determined using ^{1}H NMR spectra.

The nearly quantitative conversion of both PS-NB and PEO-NB MM can be confirmed from ^{1}H NMR spectra (Figure 2a and Figures S8−S10) where the signals (6.15−6.28 ppm) of protons on the C═C bonds of NB end groups were absent for all the BBCP. At the same time, signals at 5.04−5.38 ppm (Figure 2a and Figure S8) from protons of opened C═C bonds indicated successful polymerization of norbornene backbone. ^{13}C NMR spectra of BBCP are provided in the Supporting Information as Figures S11−S13. In addition, we were able to verify that nearly all PS-NB MMs were converted into brush polymer after 20 min of reaction. This was accomplished by acquiring the ^{1}H NMR spectrum of first block (Figure S14) polymerized via ROMP using PS-NB of similar molecular weight (2.9 kg/mol). The second MM, PEO-NB, was added after 20 min reaction of the first MM (PS-NB) and initiated the polymerization of the second MM, affording PS-*b*-PEO BBCP for the study.

Bulk Sample Preparation. BBCP was dissolved in anhydrous DCM as 2 wt % solution and drop-cast on glass under a nitrogen atmosphere on a flat stage. After the solvent was evaporated, the dried film was subjected to thermal annealing under vacuum at 120 °C for 12 h. Longer annealing time did not seem to improve the morphology.

RESULTS AND DISCUSSION

BBCP Synthesis and Characterization. We synthesized a family of PS-*b*-PEO BBCPs with volume fraction of PEO block (f_{PEO}) varying from 22% to 81% and with different PEO side chain lengths (M_n ~ 2.0 and 5.0 kg/mol) following reported procedures.[19,43,48,49] The chemical compositions of the obtained BBCPs were determined using ^{1}H/^{13}C NMR data (Figure 2a and Figures S8−S13) and FT-IR spectra (Figure S15). Figure 2a shows a representative ^{1}H NMR spectrum of PS-*b*-PEO BBCP, where the signals of 6.5−7.2 ppm are ascribed to PS phenyl groups and 3.6−3.8 ppm for protons of PEO side chains. The mass ratio of PS and PEO blocks was calculated according to the corresponding molar ratio as determined using ^{1}H NMR spectra. Subsequently, the volume ratio of PS and PEO (V_{PS}/V_{PEO}) was obtained using their approximate bulk densities (1.05 and 1.08 g/cm^3 for PS and PEO, respectively). The PEO domain volume fraction was calculated as $f_{PEO} = V_{PEO}/(V_{PEO} + V_{PS})$. The molecular weights of BBCPs were obtained using GPC MALLS. The light scattering (LS) traces of the BBCPs are provided in Figure 2b and Figure S16. Table 1 summarizes the molecular characteristics of the synthesized 2k-Y and 5k-Y series of PS-*b*-PEO BBCP.

While all 2k-Y and 5k-Y samples exhibited a monomodal peak, weak shoulders and tailing were observed in GPC traces of a few samples, such as 5k-28 and 5k-32 in Figure 2b and 2k-22 in Figure S16a. These features were observed previously for other brush polymers with high molecular weights.[35,37,39,51] The shoulders observed in GPC traces of 5k-28 and 5k-32 at the shorter elution times could be due to higher molecular weight species. The tailing observed for 5k-81, 5k-49, and 5k-32 were mainly due to low molecular weight species.[19,35,43] The low population of these "impurities" is not expected exert a significant influence on the phase behavior of the BBCP.[35,51−53]

We attempted to prepare a series of PS-*b*-PEO BBCPs with extremely short PEO chains (0.75 kg/mol). However, the

DOI: 10.1021/acs.macromol.6b01415
Macromolecules 2017, 50, 1503−1511

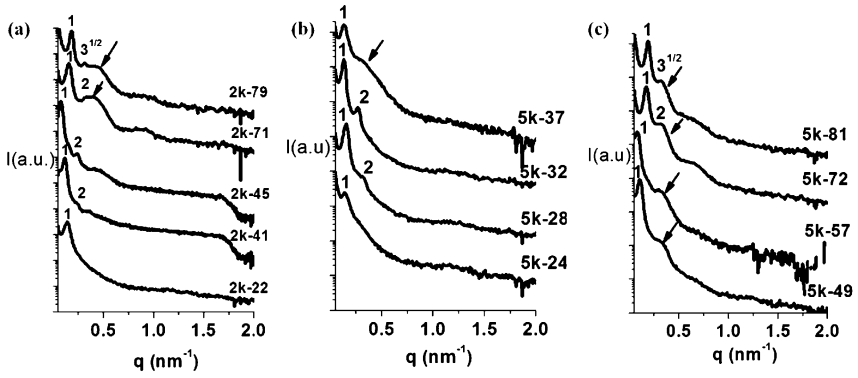

Figure 3. SAXS spectra (at room temperature) of PS-*b*-PEO BBCPs with PEO side lengths: (a) PEO $M_n \sim 2.0$ kg/mol, f_{PEO} from 22% to 79%; (b, c) PEO $M_n \sim 5.0$ kg/mol, f_{PEO} from 24% to 81%. The broad curve with an arrow is attributed to X-ray scattering from PEO crystalline lamellae.

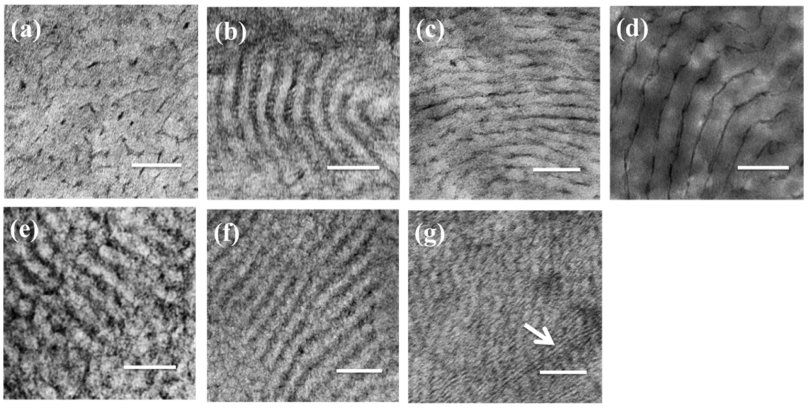

Figure 4. TEM images of cryo-microtomed PS-*b*-PEO BBCPs: (a) a disordered morphology in 2k-22; (b–e) asymmetric lamellae in (b) 2k-71, (c) 5k-28, (d) 5k-32, and (e) 5k-72; highly asymmetric BBCPs (f) 5k- 81 and (g) 2k-79. Ruthenium tetroxide (RuO_4) was used as the staining agent to improve the contrast between PS (bright area) and PEO (dark area) domains; all scale bars correspond to 100 nm. The arrow in (g) points to a region where PEO crystalline lamellae can be identified in the PEO-rich BBCP.

synthesis of the BBCPs containing PEO of 0.75 kg/mol was poorly controlled, possibly due to the rapid polymerization kinetics of small PEO-NB MMs with short side chain lengths. The GPC traces (Figure S16b) of the resulting samples show multiple peaks, indicating that multiple species in fact exist in those samples. Therefore, we did not include discussion of the morphology of these BBCPs in the text even if they showed strong phase separation and well-ordered nanostructures (Figure S17 and Table S2). Despite the exclusion of 0.75k-Y system from our discussion and conclusions, the preparation of 5k-Y and 2k-Y PS-*b*-PEO BBCPs was generally under control, and the samples were suitable for subsequent morphology studies.

BBCPs Morphology Transition. The morphologies of PS-*b*-PEO BBCPs in the bulk state were measured with SAXS (Figure 3) as well as complementary TEM analysis (Figure 4) of cryo-microtomed samples. The domain spacing (*d*-spacing) was calculated using $d = 2\pi/q^*$ for each primary scattering peak and listed in Table 1. All samples showed sharp primary scattering signals, suggesting strong phase segregation between the PS and PEO domains.

A disordered morphology ($f_{PEO} \approx 22\%$) was observed (Figure 4a), in which short and irregular shaped PEO domains were dispersed within the PS matrix. In this sample, the BBCP exhibited strong phase segregation but did not form a well-defined periodical structure such as lamellae or hexagonal packed cylinders. The SAXS spectra (Figure 3a) only show strong primary peak without high order reflections. Annealing for longer times or at higher temperature did not improve the regularity of packing. The formation of such strongly segregated but disordered morphology may result from a highly asymmetric volume fraction coupled with irregular interface curvature.

As f_{PEO} increased, we noticed that the morphology transition more depended on the variation of f_{PEO} rather than PEO side chain length (Figure 3). PS-*b*-PEO BBCP appeared to arrange into well-ordered lamellae at approximate equal volume fraction ($f_{PEO} \sim 0.5$) similar to other symmetric PS-*b*-PLA brush polymer systems.[18] Asymmetric lamellar structures were observed with f_{PEO} as low as 28% or as high as 71% in 5k-Y series. SAXS spectra of samples 2k-71, 5k-28, 5k-32, and 5k-72 reveal the ratios of q^*:q_2 = 1:2 and are consistent with TEM analysis (Figure 4b–e).

TEM images of highly asymmetric PS-*b*-PEO BBCPs, for example, 5k-81 (Figure 4f), show some evidence of parallel cylindrical or lamellar morphology patterns, while 2k-79 (Figure 4g) does not reveal clear morphology information due to the high crystallinity of PEO block and the low staining contrast between PS and PEO domains. Although TEM images have limitations for determining sample morphology, SAXS profiles with a characteristic high order reflection ratio of q^*:q_2 = 1:$\sqrt{3}$ (Figure 3a,c) indicate that in fact 5k-81 and 2k-79 exhibit cylindrical morphology at bulk state. Temperature-

DOI: 10.1021/acs.macromol.6b01415
Macromolecules 2017, 50, 1503–1511

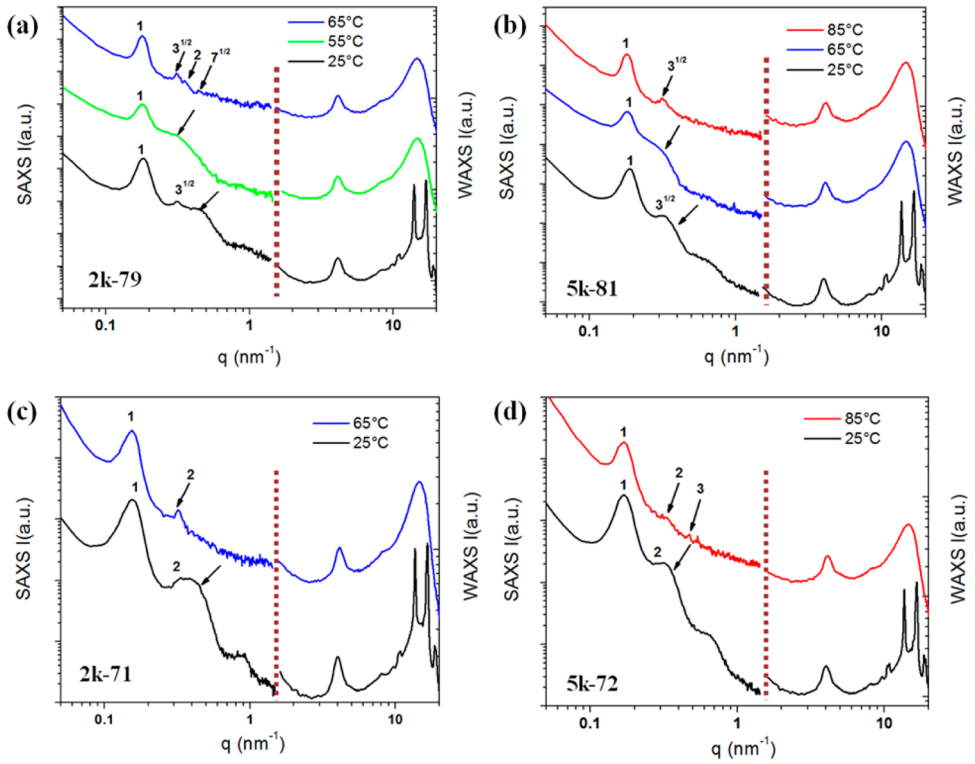

Figure 5. Temperature-controlled SAXS and WAXS 1-D profiles of BBCPs containing high volume fractions of PEO: (a) 2k-79, (b) 5k-81, (c) 2k-71, and (d) 5k-72. Higher order reflections peaks can be observed at temperature that result in a melt state of the PEO domain.

controlled SAXS profiles (Figure 5a,b) provide a more convincing result, which will be discussed later.

TEM images of PS-*b*-PEO BBCPs have relatively low contrast, especially with high f_{PEO} samples, mainly due to weak selectivity of RuO_4 staining of PS-*b*-PEO BBCP and PEO crystallization. The right bottom of Figure 4g shows the PEO crystalline lamellae with a feature size approximately 14−20 nm (labeled by a small arrow), which is consistent with appearance of broad peak at high q in SAXS spectra (Figure 3a).

Crystallization Effects. The crystallization of PEO became more apparent as f_{PEO} increased and therefore its effect on microphase segregation must be taken into consideration. A broad peak with feature size around 14−20 nm appeared in 2k-71, 2k-79, 5k-49, 5k-57, 5k-72, and 5k-81 SAXS spectra, corresponding to the thickness of PEO crystalline lamellae. To obtain a better understanding of the effect that crystallization has on the morphology transition, we compared both SAXS and WAXS spectra of four samples with high f_{PEO} (70%−80%) acquired at room temperature and above the PEO melting point (Figure 5).

In Figure 5a, at 25 °C the sample showed both sharp crystalline peaks in WAXS regime and broad peak beside the secondary high order reflection (q^*:q= 1:$\sqrt{3}$) in the SAXS regime. A series of higher order reflections (1:$\sqrt{3}$:$\sqrt{4}$:$\sqrt{7}$) consistent with a cylindrical morphology appeared as temperature increased to 65 °C, accompanied by the disappearance of PEO crystalline scattering signals in WAXS regime. The crystalline lamellae of PEO completely melt at this temperature and a well-ordered cylindrical structure was observed. Figures 5b, 5c, and 5d show similar behaviors, confirming the cylindrical (5k-81) and lamellar (2k-71 and 5k-72) morphologies of the BBCPs above the PEO melting point.

Before and after heating, the SAXS/WAXS profiles of BBCPs remained same at 25 °C. SAXS and WAXS spectra of PS-*b*-PEO BBCPs with low f_{PEO} do not show significant PEO crystallization effects on the morphology transitions. The microphase segregation of 2k-22 and 5k-28 remained approximately the same when heated within the same temperature range (Figure S18). DSC (Figure S19) analysis reveals decrease in degree of crystallization of lower f_{PEO} samples. For 2k-22, the PS-*b*-PEO BBCP had degrees of crystallization of around 50% compared to 60%−66% crystalline degree for 2k-79 and 5k-81. The slightly lower degree of crystallinity may be attributed to reduced mobility of PEO in the high-T_g PS matrix, which limited PEO side branch arrangement into crystallite lamellae.

Microphase Transition Temperature. A microphase transition temperature was observed when PS-*b*-PEO BBCPs were heated from 25 to 250 °C in a 30 °C step heating schedule with 3 min thermal equilibration at each temperature. The primary peaks in SAXS profiles of three typical PS-*b*-PEO samples (5k-28, 2k-79, and 2k-22) were fitted to Gaussian curve, and a series of full-width-at-half-maximum (FWHM) values were calculated. An abrupt change in slope determined the transition temperature in a plot of FWHM versus temperature (Figure 6).

When temperature was elevated, decreased intensities of the primary peaks and the disappearance of high order reflections was observed, indicating the decrease in degree of phase segregation.[54−56] Because the BBCP did not display long-range ordering, we followed the reference[57] and defined this temperature as microphase transition temperature T_{MST} rather than order-to-disorder transition temperature (T_{ODT}).

The T_{MST} were found to be within the range of 150−180 °C for 5k-28, 2k-79, and 2k-22 which had M_w from 280 to 350 kg/

DOI: 10.1021/acs.macromol.6b01415
Macromolecules 2017, 50, 1503−1511

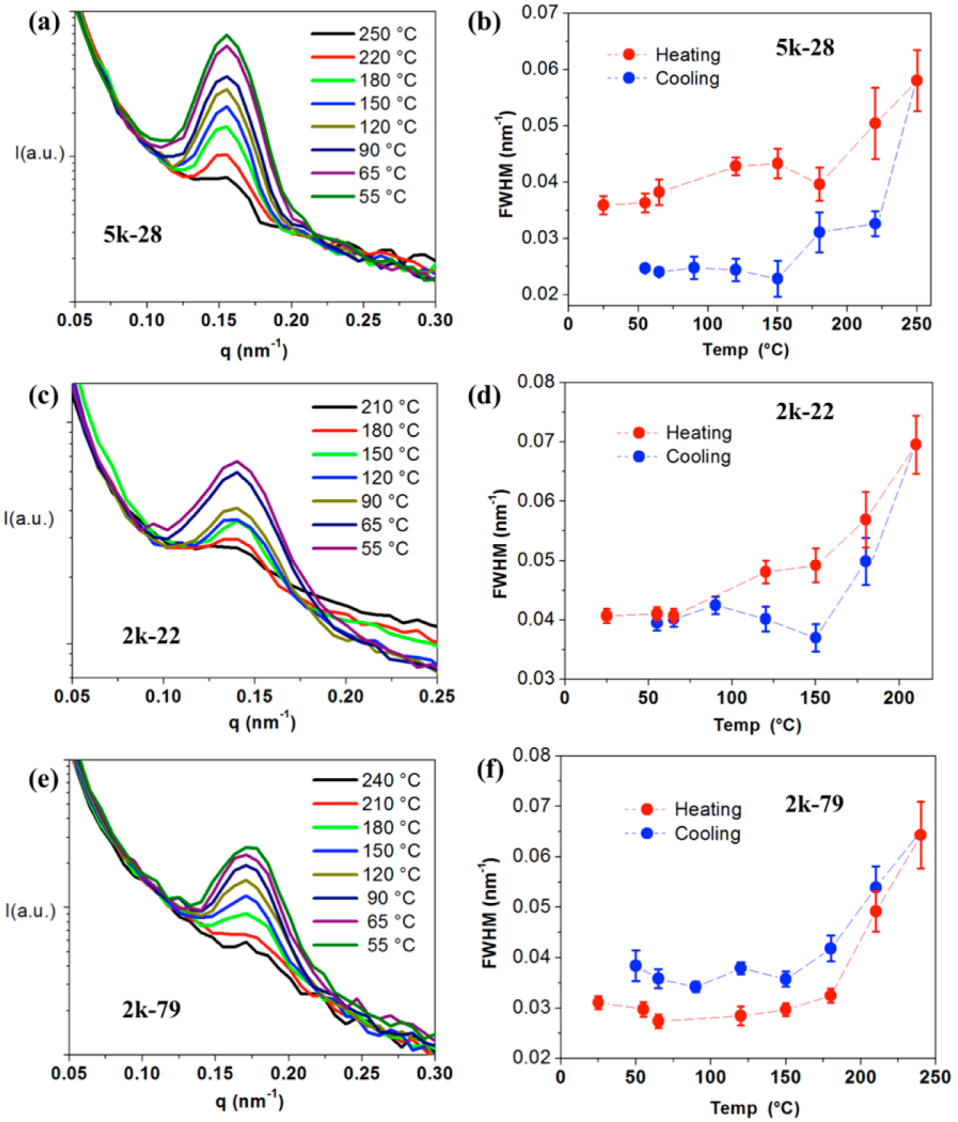

Figure 6. 1-D SAXS profiles of BBCPs: (a) 5k-28, (c) 2k-79, and (e) 2k-22 show the influence of temperature on FWHM of the primary peak. (b, d, f) FWHM as a function of temperature of BBCPs: (b) 5k-28, (d) 2k-79, and (f) 2k-22 obtained by Gaussian fitting of the primary peak.

mol. In light of these observations, the T_{MST} seemed to be relatively insensitive to volume fraction and side chain length within the molecular weight range investigated.

A few studies also investigated the effects of molecular characteristics of brush polymer on T_{ODT}. Although given the extensive variable space available in the design of brush polymers, these data sets are limited at this time. Xia and co-workers[19] found that changes in T_{ODT} of polylactide-*b*-poly(*n*-butyl acrylate) (PLA-*b*-PnBA) bottlebrush random polymers (75−85 °C) were dominated by the degree polymerization N of side chain. Dalsin et al.[46] reported that only polystyrene-*b*-(atactic) polypropylene (PS-*b*-aPP) brush block copolymer (BBCP) of low molecular weight (M_n ∼ 28.3 kg/mol) had measurable T_{ODT} of approximately 215−220 °C, while most high molecular samples did not exhibit accessible T_{ODT} below the decomposition temperature of 300 °C. In this case, the overall molecular weight affected the final T_{ODT} of BBCPs. For a typical linear BCP, the product of the Flory−Huggins parameter χ and the degree of polymerization N determines the phase transition temperature. To fully understand the role of the complex molecular characteristics of BBCPs on T_{ODT} for any one system, a comprehensive family of BBCPs with measurable T_{ODT} as a function of variable side chain lengths, backbone lengths, and block volume fractions need to be synthesized and studied.

Phase Behavior Summary. A map of PS-*b*-PEO BBCP morphology trends was constructed using side chain asymmetry versus volume fraction (f) to provide a basic understanding of the morphology for these polymers. A linear BCP phase diagram is typically plotted as the phase segregation parameter χN versus volume fraction f. Considering the complex parameters in tuning the BBCP morphology, the side chain length ratio or asymmetry was applied for the Y-axis of a phase behavior plot (Figure 7) rather than χN. It is necessary to point out that there might be several physical parameters that could also be used to illustrate the phase behavior of a BBCP. For instance, Runge et al.[33] used mole fraction of one monomer in backbone as the Y-axis for their preliminary phase diagram.

Figure 7 shows the observed morphology transitions of PS-*b*-PEO BBCPs based on our experimental results. For the reported BBCPs, a lamellar structure formed over a much wider

DOI: 10.1021/acs.macromol.6b01415
Macromolecules 2017, 50, 1503−1511

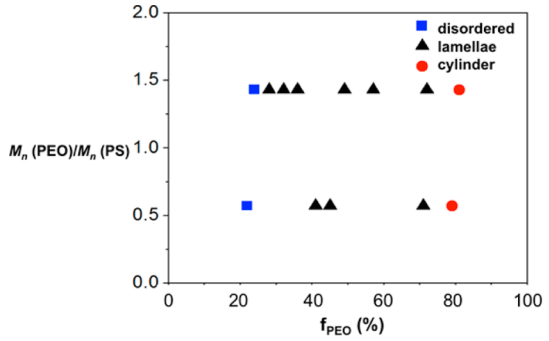

Figure 7. Summary of PS-*b*-PEO BBCP phase transition: a plot of side chain length ratio (M_n(PEO-NB)/M_n(PS-NB)) versus PEO volume fraction (f_{PEO}).

range of volume fraction when compared to linear BCP systems. The prevalence of lamellae was weakly dependent on the side chain length. This phenomenon was expected due to the existence of a highly extended backbone and the fact that the volume fraction change did not significantly affect the cross-sectional area of BBCP.[20]

The samples with high f_{PEO} yielded cylindrical morphologies with PEO acting as the matrix domain. On the other end, we noticed that in samples with low f_{PEO} the PEO domain did not exhibit cylindrical morphology; instead, they formed a "disordered" structure. This unsymmetrical morphology evolution was different from a linear PS-*b*-PEO, in which hexagonally packed PEO cylinders have been observed with $f_{PEO} \sim 33\%$.[58] Although the hexagonal packing of PEO cylinders in PS matrix was not observed in the low f_{PEO} samples, such a morphology could still be expected by tuning the molecular weight of PEO-NB MM to much smaller than that of PS-NB MM.[20,59] For instance, previous studies showed that[20] PLA cylinders were observed in a PS-*b*-PLA BBCP, in which the PLA side chains were much shorter than the PS. This asymmetry introduced a favorable curved interface, leading to the formation of well-defined PLA cylinders.

The chemical nature of side chain may also account for the interface curvature change and effect the subsequent morphology transition. Recently, the Osuji group[60] explored phase behavior of liquid crystalline brush like polymers, in which spheres, cylinders, lamellae, inverse cylinders, and spheres were observed by merely increasing weight fraction of liquid crystal. The simple occurrence of curved interface for spherical or cylindrical morphology had strong dependence on volume fraction but regardless of side chain asymmetry was apparently apart from the current understanding of BBCP system.[31,59] Such an interesting phenomenon may be due to the existence of liquid crystal group. More detailed investigations of side chain effects on BBCP morphology should be performed in the future.

CONCLUSIONS

We have demonstrated the preparation of PS-*b*-PEO BBCPs and investigated the morphology transitions as a function of side chain asymmetry and volume fraction. The molecular characteristics of side chain length and block volume fraction of 2k-Y and 5k-Y BBCPs were determined as a result of the MM synthesis approach. BBCPs showed strong phase segregation and highly asymmetric lamellae morphologies were observed with f_{PEO} ranging from 28% to 72%. Disordered and cylindrical morphologies were obtained with ultralow and high f_{PEO}, respectively. The crystallization of PEO domain interfered with the microphase segregation of PS-*b*-PEO BBCP. Consequently, higher order reflections arising from well-ordered periodic structures were readily observed in SAXS spectra measured above the PEO crystalline melting point. Upon further heating, a microphase transition temperature T_{MST} was found at 150–180 °C and was relatively independent of the side chain length and block volume fraction. An understanding of BBCP morphologies will become increasingly important as these materials find utility in the fabrication of functional materials and devices.

ASSOCIATED CONTENT

Supporting Information

The Supporting Information is available free of charge on the ACS Publications website at DOI: 10.1021/acs.macromol.6b01415.

PS-NB MM synthesis routine, BBCP volume fraction calculation, ^{1}H NMR, ^{13}C NMR, GPC traces of PS-NB, PEO-NB MMs; ^{1}H NMR and ^{13}C NMR spectra, GPC traces of PS-*b*-PEO BBCPs of different side chain length; FT-IR of 5k-Y BBCPs; temperature-controlled SAXS/WAXS of 2k-22 and 5k-57, DSC analysis of 2k-22, 2k-79, and 5k-81 (PDF)

AUTHOR INFORMATION

Corresponding Author

*(J.J.W.) E-mail: watkins@polysci.umass.edu.

ORCID

Yue Gai: 0000-0002-7430-8476

Author Contributions

Y.G. and D.-P.S. contributed equally to the manuscript.

Notes

The authors declare no competing financial interest.

ACKNOWLEDGMENTS

This work is supported by the NSF Center for Hierarchical Manufacturing at the University of Massachusetts, Amherst (CMMI-1025020). The Materials Research and Engineering Center at University of Massachusetts Amherst supported facilities used in this work.

REFERENCES

(1) Bates, F. S.; Fredrickson, G. H. Block Copolymer Thermodynamics: Theory and Experiment. *Annu. Rev. Phys. Chem.* **1990**, *41*, 525–557.

(2) Bates, F. S.; Fredrickson, G. H. Block Copolymers-Designer Soft Materials. *Phys. Today* **1999**, *52*, 32.

(3) Fredrickson, G. H.; Bates, F. S. Dynamics of Block Copolymers: Theory and Experiment. *Annu. Rev. Mater. Sci.* **1996**, *26*, 501–550.

(4) Khandpur, A. K.; Forster, S.; Bates, F. S.; Hamley, I. W.; Ryan, A. J.; Bras, W.; Almdal, K.; Mortensen, K. Polyisoprene-Polystyrene Diblock Copolymer Phase Diagram near the Order-Disorder Transition. *Macromolecules* **1995**, *28*, 8796–8806.

(5) Leibler, L. Theory of Microphase Separation in Block Copolymers. *Macromolecules* **1980**, *13*, 1602–1617.

(6) Bang, J.; Jeong, U.; Ryu, D. Y.; Russell, T. P.; Hawker, C. J. Block Copolymer Nanolithography: Translation of Molecular Level Control to Nanoscale Patterns. *Adv. Mater.* **2009**, *21*, 4769–4792.

(7) Cheng, J. Y.; Ross, C. A.; Smith, H. I.; Thomas, E. L. Templated Self-Assembly of Block Copolymers: Top-down Helps Bottom-Up. *Adv. Mater.* **2006**, *18*, 2505–2521.

DOI: 10.1021/acs.macromol.6b01415
Macromolecules 2017, 50, 1503–1511

(8) Cui, H.; Chen, Z.; Zhong, S.; Wooley, K. L.; Pochan, D. J. Block Copolymer Assembly via Kinetic Control. *Science* **2007**, *317*, 647−650.
(9) Discher, D. E.; Eisenberg, A. Polymer Vesicles. *Science* **2002**, *297*, 967−973.
(10) Ha, J. M.; Wolf, J. H.; Hillmyer, M. A.; Ward, M. D. Polymorph Selectivity under Nanoscopic Confinement. *J. Am. Chem. Soc.* **2004**, *126*, 3382−3383.
(11) Jackson, E. A.; Hillmyer, M. A. Nanoporous Membranes Derived from Block Copolymers: From Drug Delivery to Water Filtration. *ACS Nano* **2010**, *4*, 3548−3553.
(12) Klok, H. A.; Lecommandoux, S. Supramolecular Materials via Block Copolymer Self-Assembly. *Adv. Mater.* **2001**, *13*, 1217−1229.
(13) Ruzette, A. V.; Leibler, L. Block Copolymers in Tomorrow's Plastics. *Nat. Mater.* **2005**, *4*, 19−31.
(14) Tang, C.; Lennon, E. M.; Fredrickson, G. H.; Kramer, E. J.; Hawker, C. J. Evolution of Block Copolymer Lithography to Highly Ordered Square Arrays. *Science* **2008**, *322*, 429−432.
(15) Thurn-Albrecht, T.; Schotter, J.; Kästle, G. A.; Emley, N.; Shibauchi, T.; Krusin-Elbaum, L.; Guarini, K.; Black, C. T.; Tuominen, M. T.; Russell, T. P. Ultrahigh-Density Nanowire Arrays Grown in Self-Assembled Diblock Copolymer Templates. *Science* **2000**, *290*, 2126−2129.
(16) Sheiko, S. S.; Möller, M. Visualization of Macromolecules - A First Step to Manipulation and Controlled Response. *Chem. Rev.* **2001**, *101*, 4099−4123.
(17) Zhang, M.; Müller, A. H. E. Cylindrical Polymer Brushes. *J. Polym. Sci., Part A: Polym. Chem.* **2005**, *43*, 3461−3481.
(18) Gu, W.; Huh, J.; Hong, S. W.; Sveinbjornsson, B. R.; Park, C.; Grubbs, R. H.; Russell, T. P. Self-Assembly of Symmetric Brush Diblock Copolymers. *ACS Nano* **2013**, *7*, 2551−2558.
(19) Xia, Y.; Olsen, B. D.; Kornfield, J. A.; Grubbs, R. H. Efficient Synthesis of Narrowly Dispersed Brush Copolymers and Study of Their Assemblies: The Importance of Side Chain Arrangement. *J. Am. Chem. Soc.* **2009**, *131*, 18525−18532.
(20) Bolton, J.; Bailey, T. S.; Rzayev, J. Asymmetric Bottlebrush Block Copolymers. *Nano Lett.* **2011**, *11*, 998−1001.
(21) Byun, M.; Bowden, N. B.; Lin, Z. Hierarchically Organized Structures Engineered from Controlled Evaporative Self-Assembly. *Nano Lett.* **2010**, *10*, 3111−3117.
(22) Cheng, C.; Qi, K.; Khoshdel, E.; Wooley, K. L. Tandem Synthesis of Core-Shell Brush Copolymers and Their Transformation to Peripherally Cross-Linked and Hollowed Nanostructures. *J. Am. Chem. Soc.* **2006**, *128*, 6808−6809.
(23) Huang, K.; Rzayev, J. Well-Defined Organic Nanotubes from Multicomponent Bottlebrush Copolymers. *J. Am. Chem. Soc.* **2009**, *131*, 6880−6885.
(24) Kang, Y.; Walish, J. J.; Gorishnyy, T.; Thomas, E. L. Broad-Wavelength-Range Chemically Tunable Block-Copolymer Photonic Gels. *Nat. Mater.* **2007**, *6*, 957−960.
(25) Miyake, G. M.; Weitekamp, R. A.; Piunova, V. A.; Grubbs, R. H. Rapid Self-Assembly of Brush Block Copolymers to Photonic Crystals. *J. Am. Chem. Soc.* **2012**, *134*, 14249−14254.
(26) Sveinbjornsson, B. R.; Weitekamp, R. A.; Miyake, G. M.; Xia, Y.; Atwater, H. A.; Grubbs, R. H. Rapid Self-Assembly of Brush Block Copolymers to Photonic Crystals. *Proc. Natl. Acad. Sci. U. S. A.* **2012**, *109*, 14332−14336.
(27) Djalali, R.; Li, S. Y.; Schmidt, M. Amphipolar Core-Shell Cylindrical Brushes as Templates for the Formation of Gold Clusters and Nanowires. *Macromolecules* **2002**, *35*, 4282−4288.
(28) Tang, C.; Dufour, B.; Kowalewski, T.; Matyjaszewski, K. Synthesis and Morphology of Molecular Brushes with Polyacrylonitrile Block Copolymer Side Chains and Their Conversion into Nanostructured Carbons. *Macromolecules* **2007**, *40*, 6199−6205.
(29) Zhang, M.; Estournès, C.; Bietsch, W.; Müller, A. H. E. Superparamagnetic Hybrid Nanocylinders. *Adv. Funct. Mater.* **2004**, *14*, 871−882.
(30) Zhang, M.; Drechsler, M.; Müller, A. H. E. Template-Controlled Synthesis of Wire-Like Cadmium Sulfide Nanoparticle Assemblies within Core-Shell Cylindrical Polymer Brushes. *Chem. Mater.* **2004**, *16*, 537−543.
(31) Chremos, A.; Theodorakis, P. E. Morphologies of Bottle-Brush Block Copolymers. *ACS Macro Lett.* **2014**, *3*, 1096−1100.
(32) Bolton, J.; Rzayev, J. Tandem RAFT-ATRP Synthesis of Polystyrene - Poly(methyl Methacrylate) Bottlebrush Block Copolymers and Their Self-Assembly into Cylindrical Nanostructures. *ACS Macro Lett.* **2012**, *1*, 15−18.
(33) Runge, M. B.; Bowden, N. B. Synthesis of High Molecular Weight Comb Block Copolymers and Their Assembly into Ordered Morphologies in the Solid State. *J. Am. Chem. Soc.* **2007**, *129*, 10551−10560.
(34) Runge, M. B.; Lipscomb, C. E.; Ditzler, L. R.; Mahanthappa, M. K.; Tivanski, A. V.; Bowden, N. B. Investigation of the Assembly of Comb Block Copolymers in the Solid State. *Macromolecules* **2008**, *41*, 7687−7694.
(35) Rzayev, J. Synthesis of Polystyrene-Polylactide Bottlebrush Block Copolymers and Their Melt Self-Assembly into Large Domain Nanostructures. *Macromolecules* **2009**, *42*, 2135−2141.
(36) Gao, H.; Matyjaszewski, K. Synthesis of Molecular Brushes By "grafting Onto" method: Combination of ATRP and Click Reactions. *J. Am. Chem. Soc.* **2007**, *129*, 6633−6639.
(37) Lanson, D.; Ariura, F.; Schappacher, M.; Borsali, R.; Deffieux, A. Comb Copolymers with Polystyrene and Polyisoprene Branches: Effect of Block Topology on Film Morphology. *Macromolecules* **2009**, *42*, 3942−3950.
(38) Lanson, D.; Schappacher, M.; Borsali, R.; Deffieux, A. Synthesis of (Poly (Chloroethyl Vinyl Ether)-G-Polystyrene) Comb-B-(Poly (Chloropyran Ethoxy Vinyl Ether)- G-Polyisoprene) Comb Copolymers and Study of Hyper-Branched Micelle Formation in Dilute Solutions. *Macromolecules* **2007**, *40*, 5559−5565.
(39) Lee, H., Il; Matyjaszewski, K.; Yu-Su, S.; Sheiko, S. S. Hetero-Grafted Block Brushes with PCL and PBA Side Chains. *Macromolecules* **2008**, *41*, 6073−6080.
(40) Runge, M. B.; Dutta, S.; Bowden, N. B. Synthesis of Comb Block Copolymers by ROMP, ATRP, and ROP and Their Assembly in the Solid State. *Macromolecules* **2006**, *39*, 498−508.
(41) Schappacher, M.; Deffieux, A. From Combs to Comb-G-Comp Centipedes. *Macromolecules* **2005**, *38*, 7209−7213.
(42) Sumerlin, B. S.; Neugebauer, D.; Matyjaszewski, K. Initiation Efficiency in the Synthesis of Molecular Brushes by Grafting from via Atom Transfer Radical Polymerization. *Macromolecules* **2005**, *38*, 702−708.
(43) Xia, Y.; Kornfield, J. A.; Grubbs, R. H. Efficient Syntheses of Brush Polymers via Living Ring Opening Metathesis Polymerization of Macromonomers. *Macromolecules* **2009**, *42*, 3761−3766.
(44) Cheng, C.; Khoshdel, E.; Wooley, K. L. ATRP from a Norbornenyl-Functionalized Initiator: Balancing of Complementary Reactivity for the Preparation of α-Norbornenyl Macromonomers/ω-Haloalkyl Macroinitiators. *Macromolecules* **2005**, *38*, 9455−9465.
(45) Patton, D. L.; Advincula, R. C. A Versatile Synthetic Route to Macromonomers via RAFT Polymerization. *Macromolecules* **2006**, *39*, 8674−8683.
(46) Dalsin, S. J.; Rions-Maehren, T. G.; Beam, M. D.; Bates, F. S.; Hillmyer, M. A.; Matsen, M. W. Bottlebrush Block Polmers: Quantitative Theory and Experiments. *ACS Nano* **2015**, *9*, 12233−12245.
(47) Song, D. P.; Li, C.; Colella, N. S.; Xie, W.; Li, S.; Lu, X.; Gido, S.; Lee, J. H.; Watkins, J. J. Large-Volume Self-Organization of Polymer/Nanoparticle Hybrids with Millimeter-Scale Grain Sizes Using Brush Block Copolymers. *J. Am. Chem. Soc.* **2015**, *137*, 12510−12513.
(48) Song, D. P.; Li, C.; Colella, N. S.; Lu, X.; Lee, J. H.; Watkins, J. J. Thermally Tunable Metallodielectric Photonic Crystals from the Self-Assembly of Brush Block Copolymers and Gold Nanoparticles. *Adv. Opt. Mater.* **2015**, *3*, 1169−1175.
(49) Song, D. P.; Lin, Y.; Gai, Y.; Colella, N. S.; Li, C.; Liu, X. H.; Gido, S.; Watkins, J. J. Controlled Supramolecular Self-Assembly of

DOI: 10.1021/acs.macromol.6b01415
Macromolecules 2017, 50, 1503−1511

Large Nanoparticles in Amphiphilic Brush Block Copolymers. *J. Am. Chem. Soc.* **2015**, *137*, 3771−3774.
(50) Song, D.-P.; Li, C.; Li, W.; Watkins, J. J. Block Copolymer Nanocomposites with High Refractive Index Contrast for One-Step Photonics. *ACS Nano* **2016**, *10*, 1216−1223.
(51) Kawamoto, K.; Zhong, M.; Gadelrab, K. R.; Cheng, L. C.; Ross, C. A.; Alexander-Katz, A.; Johnson, J. A. Graft-through Synthesis and Assembly of Janus Bottlebrush Polymers from A- Branch -B Diblock Macromonomers. *J. Am. Chem. Soc.* **2016**, *138*, 11501−11504.
(52) Lynd, N. A.; Hillmyer, M. A. Influence of Polydispersity on the Self-Assembly of Diblock Copolymers. *Macromolecules* **2005**, *38*, 8803−8810.
(53) Lynd, N. A.; Hillmyer, M. A.; Matsen, M. W. Theory of Polydisperse Block Copolymer Melts: Beyond the Schulz-Zimm Distribution. *Macromolecules* **2008**, *41*, 4531−4533.
(54) Leibler, L. Theory of Microphase Separation in Block Copolymers. *Macromolecules* **1980**, *13*, 1602−1617.
(55) Sakamoto, N.; Hashimoto, T. Order-Disorder Transition of Low Molecular Weight Polystyrene-Block-Polyisoprene. 1. SAXS Analysis of Two Characteristic Temperature. *Macromolecules* **1995**, *28*, 6825−6834.
(56) Khandpur, A. K.; Foerster, S.; Bates, F. S.; Hamley, I. W.; Ryan, A. J.; Bras, W.; Almdal, K.; Mortensen, K. Diblock Copolymer Phase Diagram near the Order-Disorder Transition. *Macromolecules* **1995**, *28*, 8796−8806.
(57) Mannion, A. M.; Bates, F. S.; Macosko, C. W. Synthesis and Rheology of Branched Multiblock Polymers Based on Polylactide. *Macromolecules* **2016**, *49*, 4587−4598.
(58) Kim, D. H.; Sun, Z.; Russell, T. P.; Knoll, W.; Gutmann, J. S. Organic-Inorganic Nanohybridization by Block Copolymer Thin Films. *Adv. Funct. Mater.* **2005**, *15*, 1160−1164.
(59) Fenyves, R.; Schmutz, M.; Horner, I. J.; Bright, F. V.; Rzayev, J. Aqueous Self-Assembly of Giant Bottlebrush Block Copolymer Surfactants as Shape-Tunable Building Blocks. *J. Am. Chem. Soc.* **2014**, *136*, 7762−7770.
(60) Choo, Y.; Mahajan, L. H.; Gopinadhan, M.; Ndaya, D.; Deshmukh, P.; Kasi, R. M.; Osuji, C. O. Phase Behavior of Polylactide-Based Liquid Crystalline Brushlike Block Copolymers. *Macromolecules* **2015**, *48*, 8315−8322.

DOI: 10.1021/acs.macromol.6b01415
Macromolecules 2017, 50, 1503−1511